



## Discharge processes, electric field, and electron energy in ISUAL-recorded gigantic jets

Cheng-Ling Kuo,<sup>1,2</sup> J. K. Chou,<sup>1</sup> L. Y. Tsai,<sup>1</sup> A. B. Chen,<sup>1,3</sup> H. T. Su,<sup>1,4</sup> R. R. Hsu,<sup>1,3,4</sup> S. A. Cummer,<sup>5</sup> H. U. Frey,<sup>6</sup> S. B. Mende,<sup>6</sup> Y. Takahashi,<sup>7</sup> and L. C. Lee<sup>2</sup>

Received 1 October 2008; revised 23 January 2009; accepted 3 February 2009; published 23 April 2009.

[1] This article reports the first high time resolution measurements of gigantic jets from the Imager of Sprites and Upper Atmospheric Lightning (ISUAL) experiment. The velocity of the upward propagating fully developed jet stage of the gigantic jets was  $\sim 10^7$  m s<sup>-1</sup>, which is similar to that observed for downward sprite streamers. Analysis of spectral ratios for the fully developed jet emissions gives a reduced  $E$  field of 400–655 Td and average electron energy of 8.5–12.3 eV. These values are higher than those in the sprites but are similar to those predicted by streamer models, which implies the existence of streamer tips in fully developed jets. The gigantic jets studied here all contained two distinct photometric peaks. The first peak is from the fully developed jet, which steadily propagates from the cloud top ( $\sim 20$  km) to the lower ionosphere at  $\sim 90$  km. We suggest that the second photometric peak, which occurs  $\sim 1$  ms after the first peak, is from a current wave or potential wave-enhanced emissions that originate at an altitude of  $\sim 50$  km and extend toward the cloud top. We propose that the fully developed jet serves as an extension of the local ionosphere and produces a lowered ionosphere boundary. As the attachment processes remove the charges, the boundary of the local ionosphere moves up. The current in the channel persists and its contact point with the ionosphere moves upward, which produces the upward surging trailing jets. Imager and photometer data indicate that the lightning activity associated with the gigantic jets likely is in-cloud, and thus the initiation of the gigantic jets is not directly associated with cloud-to-ground discharges.

**Citation:** Kuo, C.-L., et al. (2009), Discharge processes, electric field, and electron energy in ISUAL-recorded gigantic jets, *J. Geophys. Res.*, 114, A04314, doi:10.1029/2008JA013791.

### 1. Introduction

[2] Gigantic jets (GJs), large-scale discharges from the cloud top ( $\sim 16$ – $18$  km) to the lower ionosphere, have been reported by several ground campaigns [Pasko *et al.*, 2002; Su *et al.*, 2003; van der Velde *et al.*, 2007] and a satellite experiment [Hsu *et al.*, 2005; Su *et al.*, 2005]. On the basis of the monochrome images with a time resolution of 16.7 ms, the temporal optical evolution of the GJs typically contains three stages: the leading jet, the fully developed jet (FDJ)

and the trailing jet (TJ) [Su *et al.*, 2003]. The upward propagating leading jet may be the initial stage of the FDJ, playing a role similar to that of a stepped leader in conventional lightning. In the FDJ stage, the GJ optically links the cloud top and the lower ionosphere. The trailing jet has features similar to those of the blue jets (BJs) and propagates from the cloud tops up to  $\sim 60$  km altitude. The optical emission of the trailing jet lasts for more than 0.3 s, and the overall duration of the GJs is  $\sim 0.5$  s. No related strong lightning activity has been associated with the reported GJs. In some cases ELF signals with a positive polarity have been observed with the GJs that imply that negative charge from the cloud top is transferred to the bottom of the ionosphere [Su *et al.*, 2003]. In other cases, however, no clear ELF signature was observed [van der Velde *et al.*, 2007].

[3] Another category of upward propagating discharges from the cloud top is the blue jets [Wescott *et al.*, 1995, 2001; Lyons *et al.*, 2003], which has a lower terminal altitude compared to GJs. Petrov and Petrova [1999] was the first to propose that the blue jet develops from the leader streamer zone, and hence is filled with branching streamer channels. On the basis of the work of Petrov and Petrova [1999], Pasko and George [2002] performed a three-

<sup>1</sup>Department of Physics, National Cheng Kung University, Tainan, Taiwan.

<sup>2</sup>Institute of Space Science, National Central University, Jhongli, Taiwan.

<sup>3</sup>Institute of Space, Astrophysical and Plasma Sciences, National Cheng Kung University, Tainan, Taiwan.

<sup>4</sup>Earth Dynamic System Research Center, National Cheng Kung University, Tainan, Taiwan.

<sup>5</sup>Department of Electrical and Computer Engineering, Duke University, Durham, North Carolina, USA.

<sup>6</sup>Space Sciences Laboratory, University of California, Berkeley, California, USA.

<sup>7</sup>Department of Geophysics, Tohoku University, Sendai, Japan.

**Table 1.** Band Passes of the ISUAL Spectrophotometer and the Major Emissions in the Passing Band

SP Channel	Center Wavelength (nm)	Band Width at 50% (nm)	Major Emission Band
SP1	220	140	N <sub>2</sub> LBH
SP2	337	5.6	2PN <sub>2</sub> (0–0) 337 nm
SP3	391.4	4.2	1NN <sub>2</sub> <sup>+</sup> (0–0) 391.4 nm
SP4	687	126.7	1PN <sub>2</sub>
SP5	779	7.9	O I 777.4 nm
SP6	317.6	148.2	2PN <sub>2</sub>

dimensional fractal modeling to simulate the morphology of blue jets and blue starters. Result from their numerical work agrees well with those for the observed jet phenomena [Wescott *et al.*, 1995, 2001; Pasko *et al.*, 2002]. Recently, Raizer *et al.* [2006, 2007] pointed out that the stem of a blue jet is a leader, which is a hot plasma channel with a temperature of 1500–5000 K [Raizer, 1991, p. 365; Bondiou and Gallimberti, 1994; Aleksandrov *et al.*, 1997]. A leader is capped at its top side by the streamer zone [Raizer *et al.*, 2006, 2007]. The streamers are relatively cold filaments of plasma, and the front of the streamers is a nonlinear ionization wave where air is ionized by the electron impact processes [Raizer, 1991, p. 327, and references therein]. The current in the BJs is supplied by the leader. The gas temperature in the leader channel can be as high as 5000 K from joule heating. At such a high temperature, the associative ionization ( $O + N \rightarrow NO^+ + e^-$ ) and detachment processes ( $O + O^- \rightarrow e^- + O_2$ ) increases the electron density [Aleksandrov *et al.*, 1997] and enhances the conductivity of the leader. The high conductivity in leader transmits the high electric potential from the charge region in thunderstorm, which generates the streamers at the cap of the leaders [Raizer *et al.*, 2006, 2007]. The streamer-leader phenomena in the BJs may also present in the GJs, and the disparities between them may only in their terminal altitudes and the initiating points inside the thunderstorms.

[4] Recently, a unified model of various types of upward discharges, including BJs and GJs, has been proposed by Krehbiel *et al.* [2008]. They suggested that BJs can be triggered by the charge imbalance established by the cloud-to-ground (CG) or intracloud (IC) lightning in the storms. On the basis of the proposed model, a BJ begins as electrical breakdown between the upper charge reservoir in the thundercloud and the screening charge at the cloud top. In contrast, a GJ starts as a normal IC discharge inside the cloud, but propagates upward and escapes the cloud just as a “bolt from the blue” does. However, past observations of GJs [Pasko *et al.*, 2002; Su *et al.*, 2003; van der Velde *et al.*, 2007] were based on video-rate monochrome cameras. Thus the image data cannot resolve the electric discharges occurred inside the thunderclouds. The observations also provided no spectroscopic information and temporal resolution to discriminate the dynamic behaviors in the discharge channels that span the cloud top and the lower ionosphere.

[5] In this paper, selected gigantic jets recorded using a spaceborne instrument called Imager of Sprites and Upper Atmospheric Lightning (ISUAL) are analyzed and reported. These GJ events all featured an upward and a downward propagating photometric peak that separated in time by

~1 ms. Evidence supports the interpretation that one peak is associated with the fully developed jet and the other is from a return-stroke-like process will be presented and discussed. Using the ISUAL photometric data, we are also able to deduce the propagating velocities, the magnitude of the reduced  $E$  field and the average electron energy in the FDJ of the GJs. The reduced  $E$  field is defined as  $E/N$ , where  $E$  is the  $E$  field strength and  $N$  is the neutral density. The derived values support the existence of streamer breakdown regimes in the FDJ. From the GJ-associated radio emissions recorded by Duke University ULF/ELF system, the electric nature of the FDJ is confirmed and the origin of the ELF emissions is proposed.

## 2. Instrumentation and Observation

[6] The ISUAL payload on the FORMOSAT-2 satellite consists of an ICCD imager (Imager), a six-channel spectrophotometer (SP) and a dual-band array photometer (AP). The images reported here were obtained through a 623–750 nm filter with an image frame integration time of 29 ms. The key SP data are from channel 2 (centered at 337 nm; bandwidth 5.6 nm) and channel 3 (centered at 391.4 nm; bandwidth 4.2 nm), respectively, from N<sub>2</sub> secondary positive band (2PN<sub>2</sub>, 0–0) and N<sub>2</sub><sup>+</sup> first negative band (1NN<sub>2</sub><sup>+</sup>, 0–0). Other SP channels include the SP1 (150–280 nm), the SP4 (624–750 nm), the SP5 (centered at 777.4 nm), and the SP6 (244–392 nm). The SP1 channel detects photons from N<sub>2</sub> Lyman-Birge-Hopfield (LBH) band, the SP4 channel measures N<sub>2</sub> first positive band (1PN<sub>2</sub>) emissions, the SP6 channel is for sensing the 2PN<sub>2</sub> and 1NN<sub>2</sub><sup>+</sup> emissions and the SP5 channel is for the detection of the lightning 777.4 nm OI emissions. The bandwidths of the different SP filters are summarized in Table 1. The major emission bands in molecular nitrogen detected by ISUAL SP are listed in Table 2. The ISUAL AP contains blue (370–450 nm) and red (530–650 nm) band multiple-anode photometers. Each AP module has 16 vertically stacked PMTs with a combined field of view (FOV) of 22 deg (H) × 3.6 deg (V) [Chern *et al.*, 2003; Mende *et al.*, 2005], and senses temporal and spatial variations of emissions along the vertical direction. For an event occurring near the Earth limb 3300 km away, the vertical spatial resolution of the individual AP channel is ~12 km. The ISUAL Imager, SP and AP are coaligned at the center of their views. The ISUAL Imager and SP are bore-sighted, and their FOV is approximately 20 deg (H) × 5 deg (V).

[7] An onboard routine is initiated to process an event when the changes of the brightness sensed by the ISUAL SP exceed preset threshold values. The SP sends an event flag to the ISUAL auxiliary electronic units to move the data in the circular buffers into the hardware memory. For each event flag, ISUAL stores six consecutive frames of images, typically one frame before the trigger time and 5 frames after. The ISUAL SP samples at a constant rate 10 kHz rate at all times. For each event, ISUAL saves 25 ms of SP data before the trigger point and an additional 205 ms data after the trigger. The ISUAL AP usually samples at a rate of 20 kHz. However, 20 ms after receiving a trigger, the AP rate slows down to 2 kHz and maintains at this rate for 212 ms. The total length of AP data is 240 ms (–8 ms to 232 ms).

**Table 2.** Salient Parameters of the Major Emission Band Systems for Molecular Nitrogen

Emission Band System	Upper and Lower States	Transition Wavelength (nm)	Lifetime	Quenching Altitudes (km)
1PN <sub>2</sub>	N <sub>2</sub> (B <sup>3</sup> Π <sub>g</sub> ) → N <sub>2</sub> (A <sup>3</sup> Σ <sub>u</sub> <sup>+</sup> )	478–2531 <sup>a</sup>	6 μs <sup>b</sup>	67 <sup>c</sup>
2PN <sub>2</sub>	N <sub>2</sub> (C <sup>3</sup> Π <sub>u</sub> ) → N <sub>2</sub> (B <sup>3</sup> Π <sub>g</sub> )	268–546 <sup>a</sup>	50 ns <sup>d</sup>	30 <sup>e</sup>
LBH N <sub>2</sub>	N <sub>2</sub> (a <sup>1</sup> Π <sub>g</sub> ) → N <sub>2</sub> (X <sup>1</sup> Σ <sub>g</sub> <sup>+</sup> )	100–260 <sup>a</sup>	56 μs <sup>b</sup>	84 <sup>f</sup>
1NN <sub>2</sub> <sup>+</sup>	N <sub>2</sub> <sup>+</sup> (B <sup>2</sup> Σ <sub>u</sub> <sup>+</sup> ) → N <sub>2</sub> <sup>+</sup> (X <sup>2</sup> Σ <sub>g</sub> <sup>+</sup> )	286–587 <sup>a</sup>	63 ns <sup>b</sup>	48 <sup>e</sup>

<sup>a</sup>The wavelength range of the band emissions is taken from *Lofthus and Krupenie* [1977].

<sup>b</sup>The middle values of the lifetime, inverse of the Einstein coefficient ( $A_k$ ), for the major vibrational levels of the upper state of the band system [*Gilmore et al.*, 1992] are adopted.

<sup>c</sup>At this quenching altitude, the collisional quenching rates of 1PN<sub>2</sub> with molecular nitrogen and oxygen are  $1.6 \times 10^{-11}$  and  $1.5 \times 10^{-10}$ , respectively [*Piper*, 1992].

<sup>d</sup>The lifetime of 2PN<sub>2</sub> is from *Vallance-Jones* [1974].

<sup>e</sup>The collisional quenching rates with N<sub>2</sub> and O<sub>2</sub> for 2PN<sub>2</sub> are  $1.12 \times 10^{-11}$  and  $2.85 \times 10^{-10}$ ; they are  $4.53 \times 10^{-10}$  and  $7.36 \times 10^{-10}$  for 1NN<sub>2</sub><sup>+</sup> [*Pancheshnyi et al.*, 1997].

<sup>f</sup>For LBH N<sub>2</sub>, the collisional quenching rates with N<sub>2</sub> and O<sub>2</sub> are  $2.2 \times 10^{-11}$  and  $4.3 \times 10^{-10}$  [*Marinelli et al.*, 1989, Table 1].

[8] FORMOSAT-2 is a Sun-synchronous satellite with 14 daily revisiting orbits. The ISUAL payload globally surveys transient luminous events (TLEs) and other luminous emissions in the upper atmosphere with a side-looking view. The region covered by ISUAL FOV is  $\sim 3 \times 10^6$  km<sup>2</sup>, and is scanned from south to north in each orbit [*Chern et al.*, 2003; *Mende et al.*, 2005]. Figure 1 shows the observational geometry for an ISUAL gigantic jet recorded on 1 October 2005 1122:23.898 UT. The cloud top is assumed to be  $\sim 16$  km [*Su et al.*, 2003], only 2 km lower than the typical starting height ( $\sim 18$  km) of blue jets [*Wescott et al.*, 1995, 2001]. Ray  $\overline{SC}$  connected the ISUAL Imager (S; altitude 891 km) and the geometric center of the cloud emission C. Using the satellite orbital information, the latitude and longitude of the point C can be calculated by intersecting the ray  $\overline{SC}$  and the curve at an altitude of the assumed cloud top 16 km (the dotted line in Figure 1). The distance  $\overline{SC}$  is estimated as  $\sim 3000$  km. The geographic location of the point C is calculated to be 10.2 deg S, 177.5 deg E.

### 3. Representative GJ Event on 1 October 2005 1122:23.898 UT

[9] The image sequence of a GJ recorded on 1 October 2005 1122:23.898 UT and the associated SP signals are shown in Figure 2. Figure 2a and Figures 2b–2f are recognized as the FDJ and the TJ features, respectively, of the GJ as reported by *Su et al.* [2003]. In the first 29 ms of

the FDJ in Figure 2a, the horn-shaped GJ had a full width at half maximum (FWHM) diameter of  $\sim 5$  km below 60 km, and fanned out above 60 km altitude. As measured from the ISUAL ICCD imager, the average brightness of this gigantic jet at altitudes of  $\sim 40$ –80 km, at the time of Figure 2a, was  $\sim 0.4$ –0.8 mega-Rayleigh (MR) over the 29 ms exposure time with the brightest part at an altitude of  $\sim 70$  km. The Rayleigh is the unit for the integrated light emission rate in TLEs along the line of sight from each pixel of the ISUAL CCD imager. One Rayleigh is equivalent to  $10^6$  photons cm<sup>-2</sup>-column s<sup>-1</sup> [*Baker and Romick*, 1976].

[10] In Figures 2g–2l, the first and the second SP data peaks after the event trigger are labeled as P1 and P2, respectively. The first peak is present in the SP1 (LBH N<sub>2</sub>), SP2 (2PN<sub>2</sub>), SP3 (1NN<sub>2</sub><sup>+</sup>), SP4 (1PN<sub>2</sub>) and SP6 (2PN<sub>2</sub>, 1NN<sub>2</sub><sup>+</sup>), but not in the SP5 (OI 777.4 nm). The SP records the GJ emissions integrated over the entire FOV. Hence, we utilize the AP data to resolve the altitude evolution profile of the radiative emission as shown in Figure 3a. In Figure 3b, the expected altitude for each pixel in the imager frame can be estimated from the observational geometry of Figure 1, assuming a cloud top altitude of  $\sim 16$  km. The left and right vertical axes of Figure 3b indicate the altitude in units of km and the respective AP channel numbers 8 – 16. Figure 3c is the expanded view of the AP signal traces between  $-1.5$  and 4 ms (the dashed region in Figure 3a). In Figure 3c, the blue and the red emission curves represent the AP recorded brightness with blue and red filters, respectively, in arbitrary linear units for

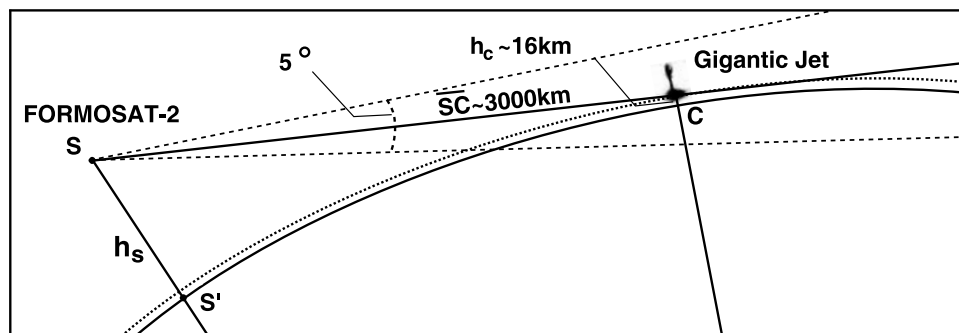


**Figure 1.** ISUAL observational geometry for the gigantic jet recorded on 1 October 2005 1122:23.898 UT, where the FORMOSAT-2 satellite S at altitude  $h_s \sim 890$  km and the geometric center C of cloud top at  $\sim 16$  km are labeled.

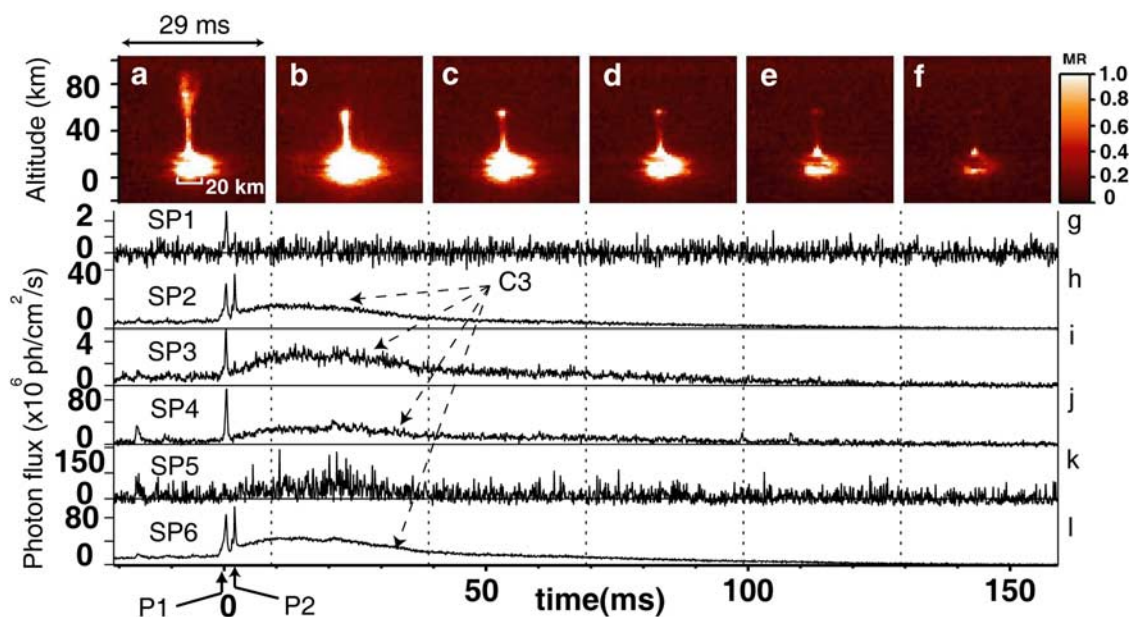


**Figure 2.** ISUAL GJ on 1 October 2005, 1122:23.898 UT. Figures 2a–2f are the time sequence images from the ISUAL Imager, and Figures 2g–2l are signal traces from the six ISUAL SP channels, where the first peak (P1) and the second peak (P2) were from the fully developed jet and a return-stroke-like process in the GJ, respectively.

each AP channels. Evidently, the first SP photometric peak (P1) in Figure 2 can be further resolved by the ISUAL AP and is the upward propagating wave in Figure 3c. The AP data indicate that the luminous pulse traveled from  $\sim 30$  km to  $\sim 90$  km. Approximately one millisecond after P1, the AP signals also indicate that the second SP photometric peak (P2) is a downward propagating wave traveled from  $\sim 50$  km to  $\sim 20$  km.

[11] Figures 3d and 3e show a detailed view of the altitude profile of the blue-filtered and the red-filtered AP data between  $-1.1$  and  $0.7$  ms relative to the GJ trigger time. The vertical resolution of each AP channel is  $\sim 12$  km at the distance of 3000 km between the GJ and the satellite. A background signal obtained by averaging AP data before the time range of interest has been subtracted from each signal. For this GJ, we choose the time range between  $-4$  and  $-3.75$  ms to obtain the background. In Figure 3d, between  $-1.05$  and  $-0.9$  ms, a weak but distinguishable luminous emission peak at altitudes of 27–39 km can be found in the AP blue channel 10. Between  $-0.9$  and  $-0.3$  ms, the blue luminous pulse shows up at altitudes of 39–51 km in the AP blue channel 11. At a time of  $-0.9$  ms, labeled by “B1,” the flat signal in two subsequent channels implies that the luminous emission peak is crossing from AP blue channel 10 to 11. The estimated error on altitude is half the channel height,  $\sim 6$  km. Hence we can identify the AP blue signals with the arrival time  $-0.9$  ms,  $-0.3$  ms,  $0.05$  ms, respectively labeled by B1, B2 and B3, were from the altitudes of 39, 51 and 63 km.

[12] For the AP red module (Figure 3e), before  $-0.6$  ms, we can discern the red emission peak at altitudes of 39–51 km in the AP red channel 11. The AP red emissions at the time of  $-0.35$ ,  $0.025$ , and  $0.35$  ms (labeled by “B2,” “B3” and “B4”) were from the altitudes of 51, 63 and 75 km. The

AP red signals preceded the AP blue signals by  $\sim 0.05$  and  $\sim 0.025$  ms for emissions from altitudes “B2” and “B3.” The estimated timing error is  $\sim 0.05$  ms. Hence, we can identify the emissions with the arrival times  $-0.9$ ,  $-0.3$ ,  $0.05$  and  $0.35$  ms were from altitudes of 39, 51, 63 and 75 km and respectively labeled them as “B1,” “B2,” “B3” and “B4.” On the basis of these data, the propagation velocities were deduced to be  $1.7$ ,  $3.6$  and  $4.2 \times 10^7$  m s $^{-1}$ , respectively. The luminous emission peak accelerates as it approaches the bottom of the ionosphere with an estimated acceleration between 2 and  $4 \times 10^{10}$  m s $^{-2}$ .

[13] As indicated by the blue photometric traces in Figure 3c,  $\sim 1$  ms after peak P1, a luminous pulse (P2) appeared to originate at altitudes of 40–50 km and traveled downward. However, because of the significant quenching under 60 km altitude for the  $1\text{PN}_2$  emission, the corresponding signal train was absent from the AP red channels. The velocity of the downward propagating pulse can be derived from the AP blue module data and is found to be  $3 \times 10^7$ – $1 \times 10^8$  m s $^{-1}$ , which is slightly higher than the velocity of the FDJs. Also within 150 ms following the photometric peak P2, a trailing jet with a mushroom-like cap appeared to propagate upward as depicted in the imager data, Figures 2b–2f. The FWHM diameter of this cap is  $\sim 8$  km, as estimated from Figure 2b. From Figure 2b, the average brightness of the TJ at altitudes in 27–62 km was  $\sim 2$  MR, with the brightest portion having  $\sim 2.8$  MR brightness in the altitude region 39–51 km. At the time of the peak P2 in Figure 2, the SP data show nearly no red emission (SP4) and thus the emissions are blue-dominated. However, after the peak P2, a slow-varying emission curve (denoted as C3 in Figure 2 and Figure 3) in SP2, SP3, SP4 and SP6 at an estimated altitude of  $< 27$  km started to rise, as shown in

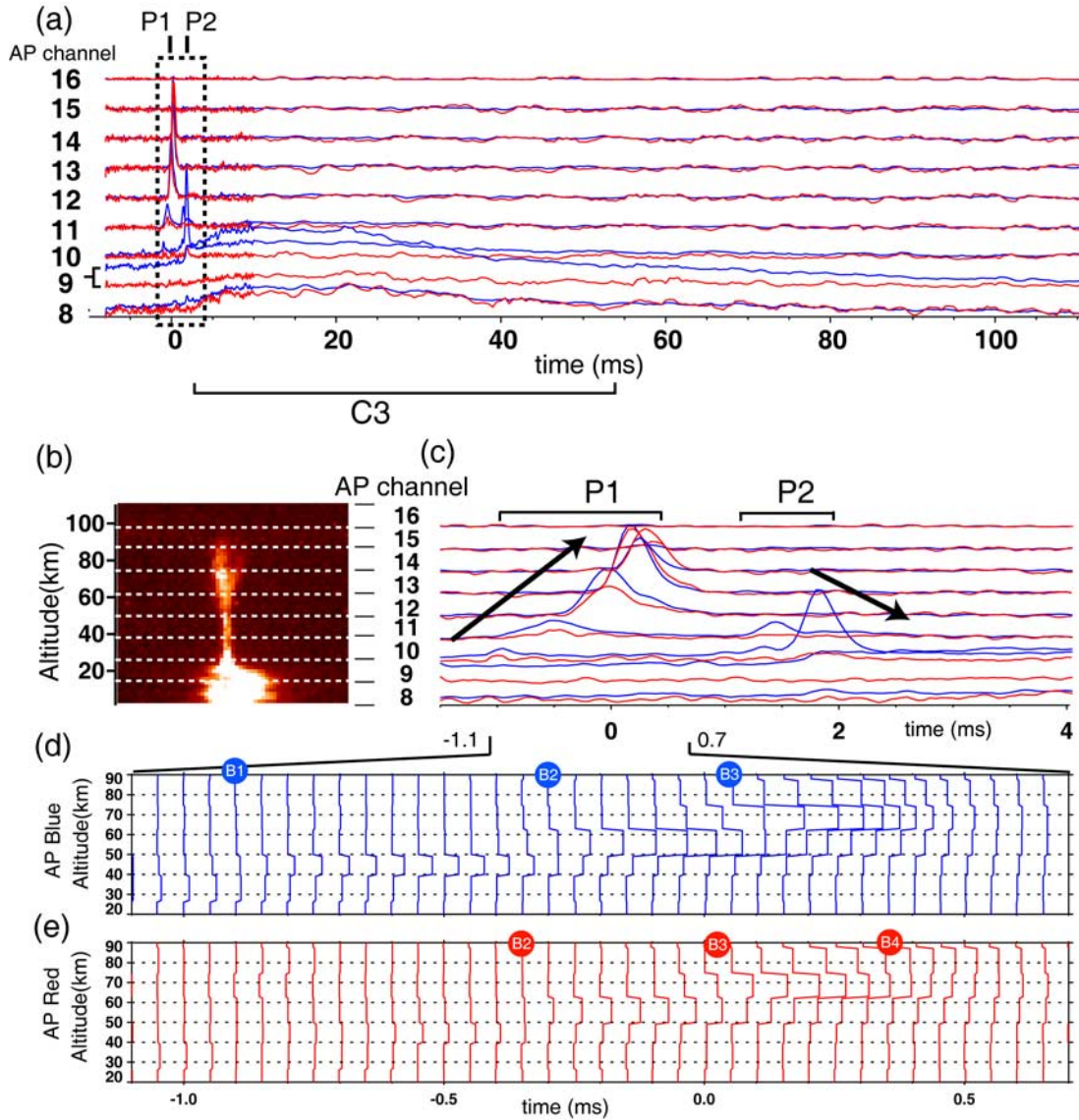


**Figure 3.** (a) The associated AP photometric data for the GJ in Figure 1. Data from the red and the blue modules are indicated by the red and the blue lines, respectively. (b) The first frame of the ISUAL Imager data for this GJ. (c) Expanded view of the AP signal traces between  $-1.5$  and  $4$  ms (the dashed rectangular in Figure 3a). The background-subtracted AP data with (d) blue filter and (e) red filter for the time ranging between  $-1.1$  and  $0.7$  ms.

Figure 3a. This indicates that most of the long-persisting emissions were from the cloud-deck level.

#### 4. Electric Field and Electron Energy in the GJs

[14] Compared with previous GJ observations [Pasko *et al.*, 2002; Su *et al.*, 2003; Hsu *et al.*, 2005; Su *et al.*, 2005; van der Velde *et al.*, 2007], ISUAL provides high temporal resolution (0.05 ms for the AP), detailed spectroscopic information, and the ability to observe blue emissions due to a higher atmospheric transmittance for satellite observations. Previous work has shown that the  $E$  field magnitudes and the average electron energies derived from the ratio SP2/SP3 ratio are consistent with the predictions of the sprite streamer model [Kuo *et al.*, 2005; Liu *et al.*, 2006]. Below we assume that most of the GJ luminous emissions

are from streamers, and analyze them using the methods discussed by Kuo *et al.* [2005].

[15] The relative response functions,  $R(\lambda)$ , for all of the ISUAL instruments have been calibrated in the preflight tests [Mende *et al.*, 2005]. Here we consider the major band emissions ( $1PN_2$ ,  $2PN_2$ ,  $N_2$  LBH and  $1NN_2^+$ ) of molecular nitrogen [Kuo *et al.*, 2007, and references therein]. The percentage of the total band emission into an ISUAL sensor unit is defined as the band percentage  $B_k(h)$  from the  $k$ th band.  $B_k(h)$  also is a function of the altitude  $h$  and can be expressed as

$$B_k(h) = \frac{\sum_{\lambda} I_k(\lambda) T(\lambda, h) R(\lambda) q_k(h) \Delta \lambda}{\sum_{\lambda} I_k(\lambda) \Delta \lambda} \quad (1)$$

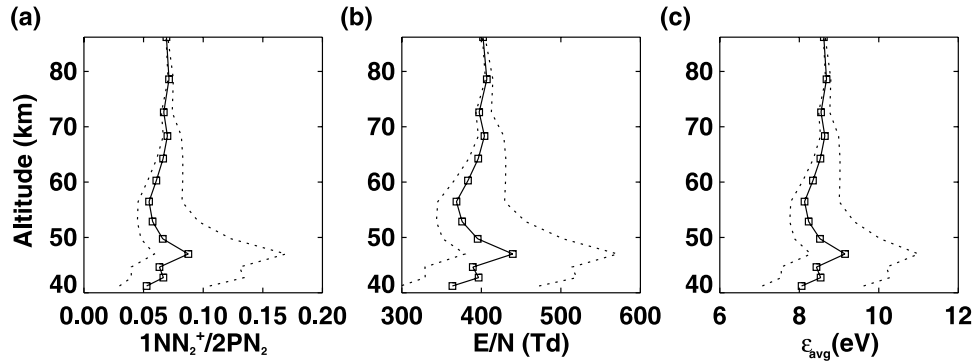


**Figure 4.** Altitudinal variation of (a) the  $1\text{NN}_2^+$  to  $2\text{PN}_2$  emission ratio, (b) the inferred reduced  $E$  field ( $E/N$ ), where  $E$  is the  $E$  field strength and  $N$  is the neutral density, and (c) the deduced average electron energy for the GJ on 1 October 2005 1122:23.898 UT. The dashed lines represent the lower and the upper bounds of these physical quantities.

where  $I_k(\lambda)$  is the intensity of emission lines in the  $k$ th band emission as a function of wavelength  $\lambda$ ,  $T(\lambda, h)$  is the atmospheric transmittance,  $R(\lambda)$  is the instrument response, and  $q_k(h)$  is the quenching ratio. The major attenuation mechanisms include  $\text{O}_2$  absorption,  $\text{O}_3$  absorption and molecular Rayleigh scattering [Kuo *et al.*, 2007, and references therein]. The quenching factor  $q_k(h)$  is defined by [Vallance-Jones, 1974]

$$\frac{1}{1 + [k_{q,N_2}N_{N_2}(h) + k_{q,O_2}N_{O_2}(h)]/A_k}$$

where  $k_{q,N_2}$  and  $k_{q,O_2}$  are the collisional quenching rates for molecular nitrogen and oxygen;  $N_{N_2}(h)$  and  $N_{O_2}(h)$  are the number densities of molecular nitrogen and molecular oxygen as a function of altitude  $h$ ;  $A_k$  is the Einstein coefficient for the  $k$ th band emission. The collisional quenching rates and Einstein coefficients for the various band emissions are given in Kuo *et al.* [2007, and references therein]. The number densities of molecular nitrogen and oxygen are calculated using the MSIS model [Hedin, 1991].

[16] We use the known band percentages of ISUAL SP2 and SP3 to infer the total band emissions in  $2\text{PN}_2$  and  $1\text{NN}_2^+$  [Kuo *et al.*, 2005, 2008]. The ratio  $1\text{NN}_2^+/2\text{PN}_2$  reflects the relative ratio of the ionization rate for  $1\text{NN}_2^+$  to the excitation rate for  $2\text{PN}_2$ . Compared with the projected rate ratio of  $1\text{NN}_2^+$  to  $2\text{PN}_2$  calculated using the ELENDF code [Kuo *et al.*, 2007], the same ratio derived from the ISUAL observed events can be used to deduce the reduced  $E$  field and the average electron energy [Kuo *et al.*, 2005]. The validity of calculating the emission intensity ratio  $1\text{NN}_2^+/2\text{PN}_2$  is justified under the steady state conditions.

[17] The altitude range of the major emissions in the streamer region of the GJ precursor is about the height of one or two AP channels ( $\sim 12$ – $24$  km) between altitudes of  $\sim 40$  to  $\sim 80$  km. The altitude uncertainty for the upward propagating luminous emissions in the fully developed stage of the GJ is about half of an AP channel,  $\sim 6$  km. Taking the possible error due to the altitude of the cloud top into account, we estimate the error on altitudes to be  $\pm 10$  km. Using the time- and altitude-resolving ISUAL AP data shown in Figure 3, the time in the SP readings (Figure 2) can be converted into the occurrence height.

The altitude-varying ratio of  $1\text{NN}_2^+/2\text{PN}_2$  is computed and shown in Figure 4a. Figures 4b and 4c present the inferred reduced  $E$  field and the average electron energy in the representative GJ, computed using the methods reported by Kuo *et al.* [2005]. The dashed lines in Figure 4 mark the maximum and minimum values of the derived quantities, after taking the possible error of  $\pm 10$  km on altitudes into account. In the streamer region of this GJ event, the ratio ( $1\text{NN}_2^+/2\text{PN}_2$ ) is  $\sim 0.07$ . The reduced  $E$  field is thus  $\sim 394$  Td (1 Townsend =  $10^{-21}$  V-m $^2$ ) and the average electron energy is  $\sim 8.5$  eV.

[18] During the first 3-year survey (2004–2007), 13 GJs were identified from the ISUAL recorded events [Chen *et al.*, 2008]. We selected 5 GJs with clear AP and SP signals, as shown in Table 3, for detailed analyses. The observed and the deduced luminous characteristics of the selected ISUAL GJs are listed in Table 3. The brightness of the FDJ varies from 0.35–2 MR at the altitude of the cloud tops ( $\sim 20$  km) to the bottom of the ionosphere ( $\sim 90$  km). The measured brightness of the TJ is weaker (0.2–0.8 MR) in four of the five GJs. The FDJ velocity is measured from the AP data with an altitude resolution of  $\sim 12$  km and a time resolution of 0.05 ms. The GJ velocities in Table 3 are all on the order of  $10^7$  m s $^{-1}$ . The ratio of  $1\text{NN}_2^+$  to  $2\text{PN}_2$  emission is 0.07–0.27, corresponding to a reduced  $E$  field of 400–655 Td. This in turn yields the average electron energy in the FDJ streamer region to be 8.5–12.3 eV. The reduced  $E$  field and the average electron energy are significantly higher than those in the ISUAL sprites as reported by Kuo *et al.* [2005]. However, the results for the GJs are similar to those obtained from a streamer model [Liu and Pasko, 2004; Liu *et al.*, 2006]. It is a good indication that the high  $E$  field exists in the streamer tip and the magnitude of  $E$  field can exceed  $3E_k$ , where  $E_k$  is the conventional breakdown threshold field [Raizer, 1991, p. 135].

[19] The velocity of the observed FDJs is on the order of  $10^7$  m s $^{-1}$ , two orders of magnitude faster than that of the blue jets ( $\sim 10^5$  m s $^{-1}$ ) [Wescott *et al.*, 1995] but comparable to the typical downward and upward sprite streamer velocities ( $10^7$  m s $^{-1}$ ) measured by 10,000 fps imagery [McHarg *et al.*, 2007] and a multinode photometer array [McHarg *et al.*, 2002]. The highest upward sprite streamer velocity was  $1.4 \times 10^8$  m s $^{-1}$ , nearly half of the light speed. Similar

**Table 3.** Observed and Derived Physical Quantities for the Five Selected GJs

Trigger Time <sup>a</sup>	Geolocation <sup>a</sup>		ULF/ELF <sup>b</sup> Polarity	FDJ <sup>c</sup>		TJ <sup>d</sup>		FDJ <sup>e</sup>				
	Lon	Lat		H (km)	Brightness	H (km)	Brightness	H (km)	V (x1E7 m s <sup>-1</sup> )	1NN <sub>2</sub> <sup>+/2PN<sub>2</sub></sup>	eV	E/N
21 Mar 2005 1950:33.999	54.97	-12.32	N/A	25-87	0.35-1.0	25-61	0.3-0.5	50-87	2.7-5.1	N/A	N/A	N/A
1 Oct 2005 1122:23.898	-177.54	-10.22	N/A	27-87	0.4-0.8	27-62	2	39-87	1.7-4.2	~0.07	~8.5	~400
13 Dec 2005 1305:54.688	158.42	-11.11	+	23-85	0.4-1.0	23-63	0.2-0.8	33-73	1.5-4.3	~0.20	~11.7	~600
28 Feb 2006 0435:52.993	-72.68	-4.43	+	23-90	0.5-2.3	23-63	0.2-0.6	35-50	2.8	~0.20	~11.2	~585
14 Mar 2006 1633:00.609	111.40	-16.79	+	26-95	0.5-1.0	26-68	0.12	38-68	2.4-4.5	~0.27	~12.3	~655

<sup>a</sup>The geolocation (longitude and latitude) means the ground projection of the GJ events, which were calculated using the observational geometry shown in Figure 1.

<sup>b</sup>Source polarity of the sferics was inferred from the data recorded by the Duke University extremely low/ultralow frequency (ULF/ELF) radio system. The plus symbol (+) indicates that the sferics has positive polarity.

<sup>c</sup>FDJ denotes the fully developed stage of the GJ, and its estimated altitudes and brightness are in units of km and mega-Rayleigh, respectively.

<sup>d</sup>Same as footnote c, and TJ stands for the trailing jet of the GJs.

<sup>e</sup>The reduced  $E$  field and the average electron energy were calculated using the streamer optical model [Kuo *et al.*, 2005, 2007].

downward streamer velocities measured by 10,000 fps imagery and photometer array were also reported in *Stenbaek-Nielsen and McHarg* [2008]. The acceleration of the FDJ is on the order of  $10^{10}$  m s<sup>-2</sup> at altitudes of 40–70 km, which is also consistent with observed sprite streamer accelerations;  $1.8 \times 10^{10}$  m s<sup>-2</sup> for the upward streamers and  $0.5 \times 10^{10}$  m s<sup>-2</sup> for the downward streamers. [McHarg *et al.*, 2007]. Numerical streamer simulations show the propagating velocities to be around  $10^6$  m s<sup>-1</sup>, the same as that for laboratory streamers [Briels *et al.*, 2008]. However, in the fast expansion and acceleration phase of overvoltage streamers initiated in  $1.1E_k$  field, the speed of the streamers can reach  $2.2 \times 10^7$  m s<sup>-1</sup> as reported in numerical simulations [Liu and Pasko, 2004; Liu *et al.*, 2006].

[20] In Table 3, three of the five GJs were found to have associated radio emissions with a positive polarity (i.e., positive charge moving downward inside the cloud) as seen in the data recorded by the Duke University extremely low/ultralow frequency (ULF/ELF) radio system. The detected polarity ULF/ELF sferics is positive at the time of peak P1. No strong lightning emission in SP5 (lightning 777.4 nm) infer no strong stroke, which contributes no significant signal of sferics inside the cloud. It implies that currents in the FDJ stage of the GJs generate the ULF/ELF emissions. This would be the negative cloud-to-ionosphere (–CI) as proposed by *Su et al.* [2003]. In the –CI scenario, the negative streamers carry negative charges and propagate upwardly from the cloud top to the lower ionosphere in the FDJ stage of GJs.

[21] It should be noted that the apparent saturation of the images, Figures 2a–2f and Figure 3b, from the emissions associated with the lightning activity at the cloud deck level is a processing artifact. To bring out the detailed structures of the GJs, we have to set a very narrow intensity range for these images. Since even the dimmest lightning illumination substantially outshines the brightest GJs, a proper setting for the GJs will make the lightning emissions in the same image frame appear to saturate. In reality, the lightning emissions at the cloud deck level for the GJ presented in Figure 2 are weak, as it can be discerned from the associated 777.4 nm emissions in ISUAL SP channel 5.

[22] To summarize, the inferred reduced  $E$  field and the average electron energy in the fully developed jets are  $560 \pm 110$  Td and  $10.9 \pm 1.7$  eV, respectively. These values are

substantially higher than those in sprites, but are similar to those predicted by the streamer models [Liu *et al.*, 2006]. Thus, these results imply the existence of streamer tips in the FDJ stage of the GJs. The speed of upward moving fully developed jets is the same order as that of downward sprite streamers. The upward propagating luminous emissions in the FDJs (P1 in Figure 3c) are thus from streamer tips that extend about  $\sim 1$ –2 AP channels (12–24 km), as shown in Figures 3d and 3e. Sferics associated with three of the five GJs listed in Table 3 exhibited positive polarity, which supports the existence of upward moving negative streamers in the FDJ stage of GJs.

## 5. Discussion

[23] Starting as a lightning leader but escaping from the cloud top [Krehbiel *et al.*, 2008], the fully developed jet behaves similarly to the streamer-leader phase of a long spark [Bazelyan and Raizer, 2000, pp. 27–89; Bondiou and Gallimberti, 1994; Mazur *et al.*, 2000] but with very different length and time scales. The reduced  $E$  field derived from the detected photometric signal in the FDJ confirms the existence of the streamer region in the GJs. This suggests that the escaped lightning leader above the cloud top produces streamers that extend from  $\sim 30$  km to 90 km; a length which is substantially longer than the several meters for the laboratory streamers [Bazelyan and Raizer, 2000, p. 86]. Also the luminous duration of the fully developed jet, represented by the P1 photometric peak in Figures 2 and 3c, can last for several milliseconds whereas it is only tens of microsecond for the laboratory leaders [Bazelyan and Raizer, 2000, p. 86]. The associated positive polarity sferics at the time of the peak P1 also suggests that streamers carry negative charges, and thus its leader should also be negative.

[24] In contrast to an arc setting in after a laboratory spark reaches the opposite electrode in the final jump phase, the FDJ streamers of the negative leader exhibit a different behavior when they reach the ionosphere. For the GJ events in the present work, a return-stroke-like process seems to occur after the FDJ has bridged the cloud top and the lower ionosphere. From the temporal and the spatial evolution of the P2 photometric peak, Figure 2 and Figure 3c, the luminosity appeared to originate at  $\sim 50$  km altitude and propagated toward the cloud top. As the FDJ faded away, a

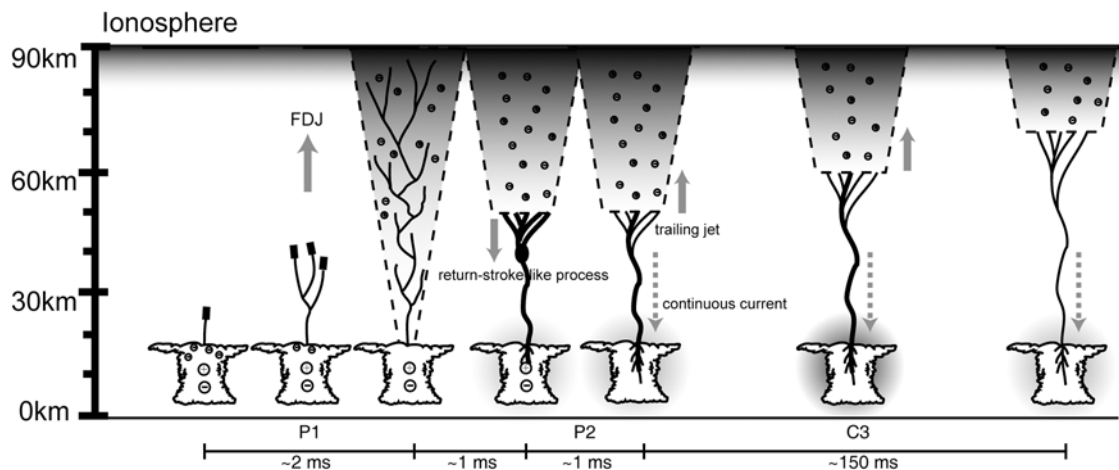


**Figure 5.** During the fully developed jet stage of the GJ, the local ionosphere boundary could be located at a much lower altitude because of the presence of the ionized channel in the FDJ. A return-stroke-like process could start at the local ionosphere boundary and extend toward the cloud top. The charge attachment process depletes the low-altitude free electrons faster, causes the ionosphere boundary to move upward, and produces the upward movement of the trailing jet.

trailing jet slowly surged upward. These characteristics all seem to point to a scenario depicted in Figure 5. When the FDJ connected to the lower ionosphere, the ionized gas in the electric path serves as the extension of the local ionosphere and resulted in a lowered local ionosphere boundary. Then positive charges flew from this lowered boundary toward the cloud top or a potential wave propagated backward along the original leader channel and produced the “return-stroke-like” phenomenon. This additional current or the strong electric field associated with the potential wave produces additional ionization along the original channel, and further heats the leader channel. Since the lower-altitude region has faster charge attachment rates, the boundary of the ionosphere gradually moves upward and eventually returns to the normal height. In this scenario, the trailing jet actually can be treated as a continuous current that connects the lower edge of the local ionosphere and the cloud top. As the attachment process moves the effective lower edge of the ionosphere upward and the continuous current persists, the contact point also moves up and the continuous current appears as an upsurging trailing jet. Since the image integration time is 29 ms and during this period the tip of the trailing jet clearly moved up, so the charge relaxation time at the 50–70 km altitude is longer than 1 ms but certainly shorter than 1 s [Pasko *et al.*, 1998; Sentman *et al.*, 2008].

[25] The trailing jet in Figures 2b–2f likely is composed of hot leader channels. The photon flux from the continuous emissions in the leader channel was below the detection limit of the AP and cannot be discerned in Figure 3a. The mushroom-like cap of the TJ may be the fan-out streamer region [Raizer *et al.*, 2006]. The leader channel is heated by the joule heating of the injected streamer currents. Because of the dominant associative ionization and the detachment processes above the critical temperature, the emission from the hot leader channels persists for at least five ISUAL Imager frames ( $> \sim 150$  ms). The TJ feature of GJs shares some interesting features with the secondary TLEs following the primary sprites [Marshall and Inan, 2007]. They are

both blue-dominated at altitudes  $< 60$  km. The luminous period of the trailing jets can be up to 0.5 s for the event reported by Su *et al.* [2003] and was  $> 0.3$  s for the ISUAL GJs studied here. For the secondary TLEs, the entire luminous duration lasts less than 0.5 s [Marshall and Inan, 2007]. The proposed generating mechanism of the secondary TLE also needs the preceding sprite to ionize the air in the altitudinal region of 50–90 km and lowers the ionospheric boundary to  $\sim 40$ –50 km.

[26] For the processes that produce the P2 pulse, an alternative possibility is the backward streamer-leader from the negative leader FDJ [Mazur *et al.*, 2000 and references therein]. If this was to happen, then the P2 pulse should be from the positive branch of the space leader [Bazelyan and Raizer, 2000, p. 85]. Therefore, the occurrence of the P2 pulse is expected to overlap in time with the P1 pulse associated with the FDJ. Since the P2 pulse trailed the P1 pulse by  $\sim 1$  ms, this implies that if the space leader did appear it must have occurred right below the original ionospheric boundary. Only below  $\sim 50$  km altitude, the luminous emissions from the backward propagating streamer-leader were intense enough and became visible to the ISUAL sensors. The backward streamer-leader fuses with the original negative leader, and together they form the new hot leader channel [Pasko, 2008, and references therein]. In laboratory studies, the negative long spark leader contains three to five steps between a 6 m rod-plane gap [Rakov and Uman, 2003, and references therein]. However, for the ISUAL recorded GJs studied in the article, at most there is only a single stepping process that radiated the P2 peak, which may imply it is a failed step formation [Pasko, 2008].

[27] The accompanying cloud emissions (C3 in Figure 2) were from the lightning activity inside or below the cloud. From Figures 2a–2f, the cloud luminous emissions for this event had complicated shapes and distinct layers. This is entirely unlike the ISUAL-observed cloud optical emissions for sprite-producing CGs [Kuo *et al.*, 2005], which have compact, symmetrical shapes since the primary emission source, the cloud to ground channel, is deeply embedded

below the cloud and the emissions are uniformly scattered by the cloud. This suggests that the GJ-associated lightning emissions originate inside the cloud and near the cloud top. Moreover, most of the ISUAL detected lightning events possess strong emission peaks in SP5 (777.4 nm), which are highly correlated with the currents in the lightning discharge channels. Since there are essentially no significant 777.4 nm emissions in these GJ events, this implies that there is no strong CG stroke associated with them and that the in-cloud lightning currents are modest at best. We believe that the cloud luminance that lasted for more than 150 ms was closely associated with the redistribution of charges which fed the continuous current in the vertical channel of the trailing jets.

[28] The gigantic jets reported in this article appear to behave like the counterpart of conventional cloud-to-ground lightning, in that they all have a leader (FDJ), a return-stroke-like process, and an ensuing continuous current. However, not all the ISUAL recorded GJs have a clearly discernible return-stroke-like signal following the FDJs. It is possible that, for the other GJs, the fully developed jet did not connect to the ionosphere and thus there is no return-stroke-like process, the luminous emissions that associated with the return-stroke-like are too dim to be detected by ISUAL instruments, or they simply belong to another category of gigantic jets. For the negative-streamer GJs, *Krehbiel et al.* [2008] pointed out that they should start as the upward intracloud discharges from the midlevel negative storm charge region. The ISUAL SP data did contain a clean peak about 17 ms before the FDJ peak (P1) and possibly some very transient flashes that followed; see the SP5 trace of the Figure 2. The luminance of this pre-FDJ peak lasted for  $\sim 1$  ms, and the other possible emission peaks were much shorter. Even though this pre-FDJ peak occurred out of the ISUAL AP data range ( $-8$  to 232 ms), channel 9 of the blue AP module did register some continuous luminance at the cloud-deck level before the occurrence of the FDJ; see Figures 3a and 3c. Since the initial propagation velocity of the leader could be very slow, it is possible that the luminance associated with it only started to cross into the next channel near the event trigger time and thus produced a near constant reading in the channel 9 of the blue AP. Hence, the data for the GJ presented in Figures 2 and 3 appears to be consistent with the GJ-generating hypothesis proposed by *Krehbiel et al.* [2008]. However, the other four GJs studied in this article showed no AP reading at the cloud-deck level and no SP pre-FDJ luminous peak, and thus the validation of the hypothesis is inconclusive.

## 6. Conclusions

[29] We report a detailed analysis of the luminous emissions in five ISUAL gigantic jets. The brightest luminous emissions from the FDJ originated in streamer heads. The velocity of the upward propagating FDJs is on the order of  $\sim 10^7$  m s $^{-1}$ , which is similar to the upward and downward sprite streamers. This suggests that the fully developed jet is also composed of many individual streamers and the FDJ is a streamer-leader process. Analysis of the spectral ratios,  $1\text{NN}_2^+/2\text{PN}_2$ , in the FDJ emissions gives a reduced  $E$  field of 400–655 Td and average electron energy of 8.5–12.3 eV.

All five ISUAL GJs studied here contain two distinct photometric peaks. The first peak was from the FDJ, which steadily propagated from the cloud top ( $\sim 20$  km) to the lower ionosphere at  $\sim 90$  km. The second photometric peak, which occurred  $\sim 1$  ms after the first peak, was likely from a current or a potential wave that originated at an altitude of  $\sim 50$  km and extended toward the cloud top. We propose that the FDJ served as an extension of the local ionosphere and produced a lowered ionosphere boundary. As the attachment processes remove the charges, the boundary of the local ionosphere moves up. The current in the channel persists and its contact point with the ionosphere moves upward, which resulted in the observed upward surging trailing jets. Imager and photometer data also indicated that the GJ-associated lightning activity is likely to be in-cloud, thus gigantic jets are not directly associated with cloud-to-ground discharges.

[30] **Acknowledgments.** Work performed at NCKU and NCU was supported in part by National Space Organization and National Science Council in Taiwan under grants 97-NSPO(B)-ISUAL-FA09-01, NSC 96-2112-M-006-003-MY3, NSC 96-2111-M-008-019, NSC 97-2111-M-006-001-MY3, and NSC 98-2111-M-008-001. Work performed at Duke was supported by NSF grants ATM-0436585, ATM-0642757, and ATM-0634661.

[31] Zuyin Pu thanks Davis Sentman and another reviewer for their assistance in evaluating this paper.

## References

- Aleksandrov, N. L., E. M. Bazelyan, I. V. Kochetov, and N. A. Dyatko (1997), The ionization kinetics and electric field in the leader channel in long air gaps, *J. Phys. D Appl. Phys.*, *30*(11), 1616, doi:10.1088/0022-3727/30/11/011.
- Baker, D. J., and G. J. Romick (1976), The Rayleigh: Interpretation of the unit in terms of column emission rate or apparent radiance expressed in SI units, *Appl. Opt.*, *15*, 1966–1968, doi:10.1364/AO.15.001966.
- Bazelyan, E. M., and Y. P. Raizer (2000), *Lighning Physics and Lightning Protection*, Inst. of Phys., Bristol, U. K.
- Bondiou, A., and I. Gallimberti (1994), Theoretical modeling of the development of the positive spark in long gaps, *J. Phys. D Appl. Phys.*, *27*, 1252–1266, doi:10.1088/0022-3727/27/6/024.
- Briels, T. M. P., E. M. van Veldhuizen, and U. Ebert (2008), Positive streamers in air and nitrogen of varying density: Experiments on similarity laws, *J. Phys. D Appl. Phys.*, *41*, 4008, doi:10.1088/0022-3727/41/23/234008.
- Chen, A. B., et al. (2008), Global distributions and occurrence rates of transient luminous events, *J. Geophys. Res.*, *113*, A08306, doi:10.1029/2008JA013101.
- Chern, J. L., R. R. Hsu, H. T. Su, S. B. Mende, H. Fukunishi, Y. Takahashi, and L. C. Lee (2003), Global survey of upper atmospheric transient luminous events on the ROCSAT-2 satellite, *J. Atmos. Sol. Terr. Phys.*, *65*(5), 647–659, doi:10.1016/S1364-6826(02)00317-6.
- Gilmore, F. R., R. R. Laher, and P. J. Espy (1992), Franck-Condon factors,  $r$ -centroids, electronic transition moments, and Einstein coefficients for many nitrogen and oxygen band systems, *J. Phys. Chem. Ref. Data*, *21*, 1005–1107.
- Hedin, A. E. (1991), Extension of the MSIS thermosphere model into the middle and lower atmosphere, *J. Geophys. Res.*, *96*, 1159–1172, doi:10.1029/90JA02125.
- Hsu, R., et al. (2005), Gigantic jet observation by the ISUAL payload of FORMOSAT-2 satellite, *Eos Trans. AGU*, *85*(47), Fall Meet. Suppl., Abstract AE31A-0151.
- Krehbiel, P. R., J. A. Riousset, V. P. Pasko, R. J. Thomas, W. Rison, M. A. Stanley, and H. E. Edens (2008), Upward electrical discharges from thunderstorms, *Nature Geosci.*, *1*(4), 233–237, doi:10.1038/ngeo162.
- Kuo, C.-L., R. R. Hsu, A. B. Chen, H. T. Su, L. C. Lee, S. B. Mende, H. U. Frey, H. Fukunishi, and Y. Takahashi (2005), Electric fields and electron energies inferred from the ISUAL recorded sprites, *Geophys. Res. Lett.*, *32*, L19103, doi:10.1029/2005GL023389.
- Kuo, C.-L., et al. (2007), Modeling elves observed by FORMOSAT-2 satellite, *J. Geophys. Res.*, *112*, A11312, doi:10.1029/2007JA012407.
- Kuo, C.-L., et al. (2008), Radiative emission and energy deposition in transient luminous events, *J. Phys. D Appl. Phys.*, *41*, 234014, doi:10.1088/0022-3727/41/23/234014.

- Liu, N., and V. P. Pasko (2004), Effects of photoionization on propagation and branching of positive and negative streamers in sprites, *J. Geophys. Res.*, *109*, A04301, doi:10.1029/2003JA010064.
- Liu, N., et al. (2006), Comparison of results from sprite streamer modeling with spectrophotometric measurements by ISUAL instrument on FORMOSAT-2 satellite, *Geophys. Res. Lett.*, *33*, L01101, doi:10.1029/2005GL024243.
- Lofthuis, A., and P. H. Krupenie (1977), The spectrum of molecular nitrogen, *J. Phys. Chem. Ref. Data*, *6*, 113–307.
- Lyons, W. A., T. E. Nelson, R. A. Armstrong, V. P. Pasko, and M. A. Stanley (2003), Upward electrical discharges from thunderstorm tops, *Bull. Am. Meteorol. Soc.*, *84*, 445–454, doi:10.1175/BAMS-84-4-445.
- Marinelli, W. J., W. J. Kessler, B. D. Green, and W. A. M. Blumberg (1989), Quenching of  $N_2(a^1\Pi_g, v' = 0)$  by  $N_2$ ,  $O_2$ ,  $CO$ ,  $CO_2$ ,  $CH_4$ ,  $H_2$ , and  $Ar$ , *J. Chem. Phys.*, *90*, 2167–2173, doi:10.1063/1.456012.
- Marshall, R. A., and U. S. Inan (2007), Possible direct cloud-to-ionosphere current evidenced by sprite-initiated secondary TLEs, *Geophys. Res. Lett.*, *34*, L05806, doi:10.1029/2006GL028511.
- Mazur, V., L. H. Ruhnke, A. Bondiou-Clergerie, and P. Lalande (2000), Computer simulation of a downward negative stepped leader and its interaction with a ground structure, *J. Geophys. Res.*, *105*, 22,361–22,370, doi:10.1029/2000JD900278.
- McHarg, M. G., R. K. Haaland, D. Moudry, and H. C. Stenbaek-Nielsen (2002), Altitude-time development of sprites, *J. Geophys. Res.*, *107*(A11), 1364, doi:10.1029/2001JA000283.
- McHarg, M. G., H. C. Stenbaek-Nielsen, and T. Kammer (2007), Observations of streamer formation in sprites, *Geophys. Res. Lett.*, *34*, L06804, doi:10.1029/2006GL027854.
- Mende, S. B., H. U. Frey, R. R. Hsu, H. T. Su, A. B. Chen, L. C. Lee, D. D. Sentman, Y. Takahashi, and H. Fukunishi (2005), D region ionization by lightning-induced electromagnetic pulses, *J. Geophys. Res.*, *110*, A11312, doi:10.1029/2005JA011064.
- Pancheshnyi, S. V., S. M. Starikovskaya, and A. Y. Starikovskii (1997), Measurements of the rates of quenching of  $N_2(C^3\Pi_u)$  and  $N_2^+(B^2\Sigma_u^+)$  states by  $N_2$ ,  $O_2$ , and  $CO$  molecules in the afterglow plasma of a nanosecond discharge, *Plasma Phys. Rep.*, *23*, 616–620.
- Pasko, V. P. (2008), Blue jets and gigantic jets: Transient luminous events between thunderstorm tops and the lower ionosphere, *Plasma Phys. Controlled Fusion*, *50*, 124050, doi:10.1088/0741-3335/50/12/124050.
- Pasko, V. P., and J. J. George (2002), Three-dimensional modeling of blue jets and blue starters, *J. Geophys. Res.*, *107*(A12), 1458, doi:10.1029/2002JA009473.
- Pasko, V. P., U. S. Inan, and T. F. Bell (1998), Spatial structure of sprites, *Geophys. Res. Lett.*, *25*, 2123–2126, doi:10.1029/98GL01242.
- Pasko, V. P., M. A. Stanley, J. D. Mathews, U. S. Inan, and T. G. Wood (2002), Electrical discharge from a thundercloud top to the lower ionosphere, *Nature*, *416*(6877), 152–154, doi:10.1038/416152a.
- Petrov, N. I., and G. N. Petrova (1999), Physical mechanisms for the development of lightning discharges between a thundercloud and the ionosphere, *Tech. Phys.*, *44*, 472–475, doi:10.1134/1.1259327.
- Piper, L. G. (1992), Energy transfer studies on  $N_2(X^1\Sigma_g^+, v)$  and  $N_2(B^3\Pi_g)$ , *J. Chem. Phys.*, *97*, 270–275, doi:10.1063/1.463625.
- Raizer, Y. P. (1991), *Gas Discharge Physics*, Springer, New York.
- Raizer, Y. P., G. M. Milikh, and M. N. Shneider (2006), On the mechanism of blue jet formation and propagation, *Geophys. Res. Lett.*, *33*, L23801, doi:10.1029/2006GL027697.
- Raizer, Y. P., G. M. Milikh, and M. N. Shneider (2007), Leader streamers nature of blue jets, *J. Atmos. Sol. Terr. Phys.*, *69*, 925–938, doi:10.1016/j.jastp.2007.02.007.
- Rakov, V. A., and M. A. Uman (2003), *Lightning: Physics and Effects*, 136 pp., Cambridge Univ. Press, Cambridge, U. K.
- Sentman, D. D., H. C. Stenbaek-Nielsen, M. G. McHarg, and J. S. Morrill (2008), Plasma chemistry of sprite streamers, *J. Geophys. Res.*, *113*, D11112, doi:10.1029/2007JD008941.
- Stenbaek-Nielsen, H. C., and M. G. McHarg (2008), High time-resolution sprite imaging: Observations and implications, *J. Phys. D Appl. Phys.*, *41*, 234009, doi:10.1088/0022-3727/41/23/234009.
- Su, H. T., R. R. Hsu, A. B. Chen, Y. C. Wang, W. S. Hsiao, W. C. Lai, L. C. Lee, M. Sato, and H. Fukunishi (2003), Gigantic jets between a thundercloud and the ionosphere, *Nature*, *423*(6943), 974–976, doi:10.1038/nature01759.
- Su, H., R. Hsu, A. B. Chen, L. Lee, S. B. Mende, H. U. Frey, H. Fukunishi, Y. Takahashi, and C. Kuo (2005), Key results from the first fourteen months of ISUAL experiment, *Eos Trans. AGU*, *86*(52), Fall Meet. Suppl., Abstract AE11A-01.
- Vallance-Jones, A. (1974), *Aurora*, pp. 118–119, D. Reidel, Dordrecht, Netherlands.
- van der Velde, O. A., W. A. Lyons, T. E. Nelson, S. A. Cummer, J. Li, and J. Bunnell (2007), Analysis of the first gigantic jet recorded over continental North America, *J. Geophys. Res.*, *112*, D20104, doi:10.1029/2007JD008575.
- Wescott, E. M., D. Sentman, D. Osborne, D. Hampton, and M. Heavner (1995), Preliminary results from the Sprites94 aircraft campaign: 2. Blue jets, *Geophys. Res. Lett.*, *22*, 1209–1212, doi:10.1029/95GL00582.
- Wescott, E. M., D. D. Sentman, H. C. Stenbaek-Nielsen, P. Huet, M. J. Heavner, and D. R. Moudry (2001), New evidence for the brightness and ionization of blue starters and blue jets, *J. Geophys. Res.*, *106*, 21,549–21,554, doi:10.1029/2000JA000429.

A. B. Chen, J. K. Chou, R. R. Hsu, C.-L. Kuo, H. T. Su, and L. Y. Tsai, Department of Physics, National Cheng Kung University, No. 1, University Road, Tainan, 70101, Taiwan. (rrhsu@phys.ncku.edu.tw)

S. A. Cummer, Department of Electrical and Computer Engineering, Duke University, Box 90291, Durham, NC 27708, USA.

H. U. Frey and S. B. Mende, Space Sciences Laboratory, University of California, 7 Gauss Way, Berkeley, CA 94720, USA.

L. C. Lee, Institute of Space Science, National Central University, No. 300, Jhongda Road, Jhongli City, Taoyuan County 32001, Taiwan.

Y. Takahashi, Department of Geophysics, Tohoku University, 6-3 Aza-aoba, Aramaki, Aoba-ku, Sendai, Miyagi 980-8578, Japan.